

DRAG REDUCTION IN TURBULENT FLOW OF POLYMER SOLUTIONS

Michael D. Graham

Department of Chemical and Biological Engineering
University of Wisconsin-Madison, Madison WI 53706-1607 USA

ABSTRACT

Progress in understanding turbulent drag reduction by polymer additives has recently been made on several fronts. The near-wall dynamics of Newtonian turbulence is becoming better understood. Detailed computations of complex flows of model polymer solutions are now possible. Insights into the effects of viscoelasticity have been gained from a number of important model flows, and the understanding of the dynamics of dilute polymer solutions, as well as the ability to perform detailed simulations of them, is maturing. We review the advances in these fronts and illustrate their contributions to the understanding of both turbulence and drag reduction. Finally, we highlight open questions and propose a general conceptual framework that would, if validated, unify observations of drag reduction from turbulence onset to the maximum drag reduction asymptote.

KEYWORDS: Turbulence; Drag reduction; Dilute polymer solutions; Transition to turbulence; Computational fluid dynamics.

1. INTRODUCTION

In the 1940s, Toms [1, 2] and Mysels [3, 4] discovered that the addition of a small amount of a high molecular weight polymer to a liquid could dramatically reduce the pressure drop necessary to generate a given flow rate in a turbulent flow. Since then, it has been found that many other types of additives, including wormy micelle-forming surfactants, bubbles, rigid fibers and even solid spheres lead to turbulent drag reduction [5]. This “rheological drag reduction” phenomenon, sometimes known as the “Toms effect”, has found widespread application in reduction of energy losses in pipelines, has spurred intense research into reducing drag over ships and has recently gained attention for improving efficiency of so-called district heating and cooling systems, in which chilled or heated water is generated at a central location in a city and pumped to buildings in the surrounding area [6]. After six decades of research, the subject remains an active area of research, in part because of applications but also because it lies at the intersection of two complex and important fields, turbulence and rheology. The desire to better understand this phenomenon

drives research in both fields, and shedding light on drag reduction may in turn yield insights into both the dynamics of drag-reducing fluids and of turbulent flows.

Drag reduction by additives has been the subject of many review articles [7-11], book chapters [5], books [6] and symposia [12-14]. Nadolink [15] has compiled a bibliography of the drag reduction literature as of 1995, containing more than 2500 references. So why is another review article appropriate now? First, because after sixty years, there is still no comprehensive mechanistic understanding of the ways that rheology and turbulence interact, much less a single theory capturing the main features of the drag reduction phenomenon: Second, and more importantly, because the past decade or so has seen significant (in this author's opinion) progress along these lines. This article will review these recent advances, with a focus on drag reduction in dilute polymer solutions. These advances have occurred on four fronts:

- Direct numerical simulations (DNS) and computational bifurcation analyses have led to important insights into the origin of the non-linear transition to turbulence in Newtonian channel and pipe flows. These analyses also shed light on the near-wall coherent structures that are observed to be significantly modified by viscoelasticity.
- Direct numerical simulations of turbulence have become feasible in viscoelastic channel flows. Such “computational experiments” allow a more detailed inspection of velocity and stress fields than do physical experiments, as well as close control over the “rheology” of the computational fluid under consideration.
- Studies of important model flows have illuminated how these are affected by viscoelasticity, shedding light on the effects of rheology on some of the building blocks of turbulence.
- Brownian dynamics simulations of coarse-grained but nevertheless fairly detailed models of polymer molecules in solution have become commonplace. These simulations have significantly improved our understanding of polymer dynamics in flows, including models of turbulent flows.

We will try to avoid repeating here material that is in earlier reviews of drag reduction, except as necessary to lay out the key observations and ideas that have laid the groundwork for recent advances. At the end, we will briefly summarize what is now known about drag reduction in polymer solutions, try to say something about what we do not know, and present a schematic framework that might serve to organize observations ranging from the onset of turbulence to the maximum drag reduction asymptote.

2. NEWTONIAN CHANNEL FLOW

Most of the rheological drag reduction literature centers on wall-bounded flows, and most current and emerging applications are in those flows, so to set the stage for further discussion we review here the behavior of Newtonian wall-bounded flows. We will begin with some of the standard results, then describe recent advances

in the understanding of near-wall turbulent structure that may provide a foundation for a deeper understanding of drag reduction.

2.1 Basic features of the mean and fluctuations

For definiteness, we focus here on pressure-driven channel flow, with average wall shear stress τ_w , of a fluid with dynamic viscosity μ , density ρ and kinematic viscosity ν . The mean flow is in the x -direction, the wall-normal direction is y and the spanwise direction is z . The mean velocity is $U(y)$, and the streamwise, wall-normal, and spanwise velocity fluctuations are u, v , and w or u_1, u_2 and u_3 , respectively. Ensemble averages are denoted with angle brackets. The channel half-height is H , and defines the geometric or “outer” length scale of the flow. We can construct an “inner” length scale as follows. Far from the wall, we take the momentum transport to be independent of viscosity — all momentum is transferred by Reynolds stresses. The characteristic, or “friction”, velocity associated with these stresses, u_τ satisfies $\tau_w = \rho u_\tau^2$. A new length scale is then given by $l_w = \nu/u_\tau$. Quantities expressed in terms of these scales, called “wall units” are denoted with a superscript $+$; for example, the distance from the wall, scaled by this inner scale, is denoted y^+ . The friction Reynolds number $Re_\tau = u_\tau H/\nu$ is simply the distance from the wall to the channel centerline, expressed in wall units.

At high Reynolds number, only the region of flow very near the wall is expected to be affected by viscosity. In particular, away from the wall, the mean velocity *gradient* is expected to be independent of viscosity. On the other hand, far from the centerline, the velocity gradient is expected to be independent of H . If there is a region that satisfies both of these conditions, the mean velocity profile $U(y)$ there must satisfy $U/u_\tau = A \log y^+ + B$. Indeed, for $y^+ \gg 30$ (but still far from the centerline), this equation can be well-fit to experimental data for turbulent flow, with $A \approx 2.5$ and $B \approx 5.5$ [16] — the region where this holds is called the *inertial sublayer* or *log layer*. For $y^+ \ll 5$, in the *viscous sublayer*, viscous effects dominate and $U/u_\tau = y^+$. These two formulas intersect at $y^+ \approx 12$. The region where neither of these equations hold, $5 \approx y^+ \ll 30$ for Newtonian flow, is called the *buffer layer* - this intermediate region turns out to play a central role in turbulence production and in polymer drag reduction, as further described below. Data for $U(y)/u_\tau$ vs. y^+ for channels and pipes collapse reasonably well onto a single curve for data over a wide range of Reynolds numbers, implying their independence from the outer scale H and thus indicating an approximate universality of the near wall mean flow behavior.

We turn now from the mean flow to the fluctuations. The rate of production of turbulent kinetic energy $k = \langle \rho u_i u_i / 2 \rangle$ peaks in the buffer layer, very close to $y^+ = 12$ independent of Reynolds number [17]. The streamwise fluctuations are significantly larger than the spanwise and wall normal fluctuations, and for $Re_\tau \ll 1000$ all of the velocity fluctuations $\langle u_i^2 \rangle$ peak in the *wall region* $y^+ < 100$, as does $\langle uv \rangle$. Despite the fact that the turbulence production peaks at $y^+ \approx 12$ independent of Re_τ , the velocity fluctuations themselves do not scale only with wall variables [18, 19]. The maxima in these quantities move away from the wall (in wall units) with increasing Re_τ ; in particular the distance from the wall where the Reynolds shear stress $-\langle \rho uv \rangle$ peaks is at

approximately $2Re_\tau^{1/2}$ for Re_τ up to at least 5000 [18]. Normalized with the turbulent kinetic energy, however, the fluctuations remain nearly constant in the log layer — there is approximate self-similarity here and the flow is locally very much like a homogeneous turbulent shear flow [17].

2.2 Coherent structures and self-sustaining processes

To this point we have not touched on the spatial structure and time dependence of turbulence at all, other than to split the velocity into mean and fluctuating parts. But what is the spatial and temporal nature of these fluctuations? Are they featureless random fields? A simple argument shows us otherwise [20]. If u and v are uncorrelated, the Reynolds shear stress $-\langle\rho uv\rangle$ would be zero. But in a turbulent channel flow, most of the xy -momentum transport outside the viscous sublayer is due to this stress, which peaks in the near-wall region, in or just beyond the buffer layer. Therefore, u and v must be correlated in a turbulent channel flow, and the fact that this correlation is largest in the wall region suggests the existence of highly organized motions, or “coherent structures”, in this region. This argument is amply supported by many observations, both from physical and computational experiments. A very brief summary of what is clear about these motions, largely following the review article of Robinson [20], is as follows:

- The viscous sublayer, buffer and outer regions have coherent motions with distinct structures.
- The viscous sublayer is dominated by streamwise “streaks” of fast and slow moving fluid. These are transient, highly elongated in the streamwise direction and have a spanwise wavelength of approximately $100 l_w$.
- The dominant structure of the buffer layer is pairs of staggered quasi-streamwise vortices [21-23]. It is these structures, which convect slow moving fluid away from the wall and faster moving fluid toward it, that set the $100 l_w$ spacing of the streaks in the sublayer. Experimental observations for Re_τ between about 10^2 and 10^4 show that this spacing is universal, independent of friction Reynolds number [18]. Using a conditional sampling technique, Jeong *et al.* [23] explicitly educed such structures from DNS of turbulent channel flow, with characteristic scales $L_x^+ \approx 350$, $L_y^+ \approx 40$, $L_z^+ \approx 100$.
- Horseshoe-shaped (hairpin, Λ) vortical structures are present, but their importance seems controversial. They do not seem to predominate in the buffer region, which as noted above is dominated by streamwise vortices with a universal size, but do seem to be important in the log region and in the core of the flow [24].
- Very large scale structures, with streamwise scales of $5H$ – $15H$, are also present (see, e.g. [25]) — these present a challenge for simulations, since a very large flow domain is required to capture them [26].

The recognition of the existence and importance of these coherent structures leads immediately to many questions. One specific one might be whether the horseshoe structures are independent of the quasi-streamwise vortices, or whether one

is driven by the other. More broadly we might ask: How do we precisely define what a “coherent structure” is? Which structures are dominant? How are they sustained? Are they intrinsic to turbulence or can they exist in isolation, without the full-scale stochasticity of turbulence? And how does the *dynamics* of these structures relate to full scale turbulence? These questions form important themes in modern turbulence research; reference [27] collects articles reflecting a number of approaches to them, focusing on the question of how near-wall turbulence sustains itself. Because turbulence production peaks in the buffer layer, and because the effects of polymer show up first in that region, we focus on recent advances in the understanding of the quasi-streamwise vortex motions that predominate there.

Swearingen and Blackwelder [28] experimentally examined the stability of Görtler vortices (whose cores are nominally purely streamwise, with no spanwise variations) as a model system. The Görtler vortices redistribute streamwise momentum, leading to a streamwise velocity that has both spanwise and wall normal inflection points. They found that the spanwise inflections are susceptible to Kelvin-Helmholtz-like instabilities that lead to turbulence. A related instability leads to the transition between axisymmetric and wavy Taylor vortices (i.e. quasi-streamwise vortices) in the circular Couette geometry. In the Görtler and Taylor-Couette flows, the underlying streamwise vortices are sustained by centrifugal force — can quasi-streamwise vortices superimposed on a mean shear sustain themselves in the absence of an external effect? Nagata [29-31] showed that the answer is yes. He used a continuation method to compute wavy Taylor vortices, and found that once a wavy vortex flow was established, the curvature of the boundaries could be taken to zero and the state would persist as a traveling wave, periodic in the streamwise and spanwise directions, moving with the mean streamwise velocity in the channel: staggered quasi-streamwise vortices are self-sustaining states in the plane Couette geometry. Such states have also been found to exist by continuation from Rayleigh-Bénard convection [32] and by adding an artificial body force to generate streamwise vortices superposed on plane Couette flow. This state becomes unstable to a fully three-dimensional state which persists when the forcing is then turned off [33].

The existence of such flows is a robust phenomenon. Similar states have been found in channel flow [33-35] and most recently in pipe flow [36], and this general class of flows has been dubbed “exact coherent states”, or ECS. In the absence of external forcing, these states arise via saddle-node bifurcations (i.e. a pair of steady states appears “from nowhere” from a point in phase space once a parameter increases beyond a certain value [37]) at Reynolds numbers slightly below the value for robust transition to turbulence seen in experiments. In Couette flow, such states first come into existence at a Reynolds number $Re \approx 128$; experimentally, transient turbulent spots are observed at $Re \gg 50$ and persistent turbulence at $Re \approx 325$ [38, 39]. In channel flow, ECS arise at $Re \approx 650$; robust turbulence sets in at about 1000. In pipe flow, the ECS arise at $Re \approx 1300$, and persistent turbulence at 2100. The onset of these states appears to be the precursor to the onset of fully developed turbulence. Structurally, these flows consist of a mean shear with superimposed wavy streamwise vortices and the associated high- and low-speed streaks in the streamwise velocity: i.e they capture the basic structure of the buffer region. We discuss below the issue of wavelength selection. Because of translation invariance in x and z (θ and z in pipe flow), if one ECS exists, then there is actually a continuous family of them, each

shifted by an arbitrary distance in x and z . These continuous symmetries have important implications for the dynamics, as discussed in [21].

The basic self-sustaining mechanism underlying the ECS is the following. A perturbation of the base flow in the form of streamwise vortices redistributes the streamwise momentum of the flow. This redistribution creates spanwise fluctuations in the streamwise velocity, the “streaks”. The spanwise inflections in the streamwise velocity profile lead to a three-dimensional Kelvin-Helmholtz-like instability. Because of the mean shear, the concentrated vorticity arising from the instability has a component in the streamwise direction, and thus develops into streamwise-staggered nearly-streamwise vortices that regenerate the streaks [40, 41].

As mentioned above, Newtonian buffer layer structure has a distinctive spanwise wavelength of ~ 100 wall units. In Poiseuille flow, it has recently been shown that the optimal spanwise wavelength of the ECS (the wavelength at which the onset Reynolds number is lowest) is 105.5 wall units, [35]. The agreement with x and y scales is also good: $L_x^+ = 274$ and $L_y^+ (= Re_\tau) = 39$ for the optimal structure. As noted above, the quasi-streamwise vortices educed from DNS data [23] have $L_x^+ \approx 350, L_y^+ \approx 40, L_z^+ \approx 100$. Jiménez and co-workers [42, 43] have used DNS to show that the turbulence can be maintained in a “minimal” channel with dimensions as small as $L_x^+ \approx 250\text{--}350, L_y^+ \approx 200, L_z^+ \approx 100$, and that the features in the region $y^+ \lesssim 40$ matched well the features of the full turbulent buffer layer. Furthermore, recent unpublished results (Stone, Waleffe and Graham, 2003) show that the peak in turbulent kinetic energy production occurs at $y^+ = 12$, in quantitative agreement with DNS results [17]. Because they are traveling waves rather than chaotic solutions, the ECS can be viewed as being “more minimal” than the minimal channel flow solution. It seems likely that they are the saddle-points in phase space around which the strange attractor [44] of the minimal channel flow is organized. This view is supported by recent simulations of Kawahara and Kida [45] and Toh and Itano [46], who have shown a clear relationship between minimal channel turbulence and underlying traveling wave structures.

The close correspondence in length scales between buffer layer structure, minimal channel structure and the optimal Poiseuille flow ECS suggests a non-linear “marginal stability” model for buffer layer turbulence: independent of Re_τ , the buffer layer behavior adjusts itself to remain at the critical size for self-sustainment of an ECS. This model is further supported by recent work of Jiménez and co-workers [42, 47]. Using DNS modified with a filtering procedure, they found that the buffer layer behavior persists when events further from the wall are filtered out, and that with appropriate filtering a fully turbulent flow could be reduced to a pure traveling wave quasi-streamwise vortex pattern localized near the wall. By varying the distance from the wall at which fluctuations began to be filtered, it was shown that the structures further from the wall arise from instabilities of this state. The existence of the ECS shows unambiguously that, independent of any other processes that might be going on in a flow, the Navier-Stokes equations support *autonomous* traveling waves with a staggered quasi-streamwise vortex structure superimposed on a mean shear, and the natural length scales of these structures are close to the length scales of buffer layer turbulence.

Further research is necessary to better establish the connection between ECS and full turbulent dynamics. One indication of this connection is that, although the

length scales characterizing the buffer layer behavior scale with wall units and seem to be set by the natural scales for the ECS, the details of the velocity fluctuations do have a dependence on outer variables (i.e. on Re_τ). This result is not inconsistent, however, with the autonomy of the buffer layer – it merely indicates that the outer behavior penetrates the buffer layer, affecting the statistics there.

3. TURBULENT DRAG REDUCTION

3.1 Survey of experimental observations

The literature on drag reduction in pipe or channel flow was thoroughly reviewed by Virk in 1975 [9], by which time much of the phenomenology of the effect was well-established. We summarize this phenomenology here, as well as pointing out more recent observations. To avoid repetition, some of the experimental results that are discussed only in the context of specific comparisons with simulations or with theories (Sections 3.2, 4 and 5), are not included here.

Very high molecular weight flexible polymers are the best molecular drag reducers. At sufficiently high molecular weight, concentrations in parts per million are sufficient to yield drag reduction. At these concentrations, the shear viscosity of the solution is indistinguishable from that of the solvent, although the extensional viscosity at high extension rates may be orders of magnitude larger than the polymer contribution to the shear viscosity and, more importantly, much larger than the viscosity of the solvent. The significance of extensional stresses has long been recognized (see e.g. [8]), and will be further discussed elsewhere in this article, but these can be quite difficult to measure (see [48]). Escudier *et al.* [49] have recently measured shear and extensional properties of a variety of polymer solutions, as well as drag reduction for those same solutions. The degree of drag reduction was found to correlate quite well with the extensional viscosities.

For a fresh sample of a simple non-ionic polymer such as polyethylene oxide (PEO), the friction Reynolds number (or wall shear stress) above which drag reduction is first observed in a given solvent is virtually independent of concentration, and decreases with increasing molecular weight. (The concentration-independence of onset is not universally observed, but these experiments are complicated by the fact that polymeric drag reducers are generally polydisperse, can be difficult to uniformly dissolve and degrade over time.) Berman [50] showed, by varying solvent viscosity by addition of glycerine, that the onset correlates with the turbulent *time* scale, i.e. the wall shear rate, and not the turbulent length scale ν/u_τ . This result is important as it argues against the notion that drag reduction occurs because polymer molecules are so extended at onset of drag reduction that they become comparable in size to the turbulent flow structures. Lumley had earlier used theoretical arguments as evidence toward this same conclusion [7]. Indeed, experiments show that the onset of drag reduction arises when the Weissenberg number $We = \lambda \tau_w / \eta$, formed from the product of wall shear rate τ_w / η and characteristic polymer relaxation time λ , becomes significantly greater than unity.

Drag reduction results are often represented on a Prandtl-von Karman plot, or equivalently a plot of U_{ave} / u_τ vs. Re_τ , where U_{ave} is the bulk average x -velocity. Once

Re_τ exceeds the onset condition, the slope of the data increases from the Newtonian value. This *slope increment* scales roughly with polymer concentration c as $c^{1/2}$. At sufficiently large Re_τ , however, results for all concentrations collapse onto a single curve. This curve, the so-called *Maximum Drag Reduction* (MDR) asymptote, seems essentially insensitive to polymer concentration, molecular weight or species — it is a universal feature of drag reduction by polymers. (Wormy micellar surfactant systems seem to exhibit a similar universal result, but the curve is different than for polymers [51]).

In the drag reduction regime important changes to the mean velocity profile $U(y)/u_\tau$ are observed. The viscous sublayer is unchanged, but the distance from the wall beyond which the Newtonian log-law slope applies is an increasing function of the degree of drag reduction — the inertial sublayer moves away from the wall. Correspondingly, the buffer layer connecting these regions thickens (in wall units), becoming in effect an intermediate buffer/inertial layer with an approximately logarithmic velocity profile $U/u_\tau = A_p \log y^+ + B_p$, whose slope A_p is approximately 11.7, significantly greater than the Newtonian value $A = 2.5$. Virk calls this region the *elastic sublayer*. At maximum drag reduction, this region evidently fills or nearly fills the channel.

Recall that in Newtonian flow, the buffer layer structure is dominated by wavy streamwise vortices with a spanwise wavelength $L_z^+ \approx 100$. This spacing increases monotonically and significantly with the degree of drag reduction. Donohue *et al.* [52] find that it roughly doubles as the degree of drag reduction increases to 50%. Correspondingly, the frequency of “bursts”, episodes of rapid motion away from the wall, as measured at a fixed streamwise position, significantly decreases. This is an indirect indication that the streamwise lengthscale of the drag-reduced flow is also increased during drag reduction. These observations have been corroborated by all studies that we know of, in particular the recent PIV studies of [53] and [54]. Along with the wall-normal thickening of the buffer layer observed in the mean flow profile, these results show that the presence of polymer increases the overall spatial scale of the near-wall turbulent flow structure.

The statistics of the velocity fluctuations also display significant changes upon onset of drag reduction. The streamwise fluctuations increase significantly except in the viscous sublayer/inner edge of the buffer layer, where they decrease, while the wall normal fluctuations and Reynolds shear stress decrease. In fact, consideration of the averaged momentum equation shows that despite the small contribution of the polymer to the shear viscosity of the fluid, the polymer must nevertheless be carrying a significant fraction of the average shear stress in a drag-reduced flow. The position of the maximum in streamwise fluctuation amplitude is shifted away from the wall (in wall units). When the MDR regime is approached, the Reynolds shear stress is much smaller than the Newtonian value [55], and at least one group [56] concludes, based on studies with Percol 727, a copolymer of polyacrylamide and sodium acrylamide, that the Reynolds shear stress vanishes at MDR, except very near the wall. In addition, the streamwise velocity fluctuations reach a maximum, then in the MDR regime decrease to levels close to, or even below, the Newtonian [53, 55]. This latter result in particular suggests that a different turbulence production phenomenon is occurring at MDR than at lower Reynolds numbers. Finally, PIV measurements indicate that even at high drag

reduction, streamwise streaks persist in the streamwise field, but the streak spacing is now comparable to the channel size [53]. This result corroborates earlier work [50], which noted that near maximum drag reduction, the outer scale variables become important in the scaling of the flow properties.

The above results are for a nominally homogeneous polymer solution. McComb and Rabie (e.g. [57, 58]) probed the effectiveness of polymer with injections of solution into different regions of flow, showing that significant drag reduction occurs only when the polymer reaches the near-wall region. They concluded that the polymer was effective in the region $15 < y^+ < 100$, which corresponds to the buffer layer and lower log layer.

In addition to causing drag reduction in fully turbulent flow, there is also longstanding evidence that the addition of polymer alters the process of transition to turbulence, delaying it to higher Re than in the Newtonian case [59, 60]. Escudier *et al.* [49] found that the delay in transition correlates well with extensional viscosity. Draad *et al.* [61] performed experiments in a pipe flow system that is sufficiently well shielded from natural disturbances that in the Newtonian case it yields laminar flow up to $Re \approx 60000$. With this very delicate system, these authors were able to show that what they called the “natural” transition (i.e. the one at $Re \approx 60000$ in the Newtonian case) occurs at lower Re for drag reducing polymer solutions. The authors tentatively suggested that this destabilization with respect to the very small natural disturbances in this system might arise from the effect of viscoelasticity on the developing boundary layer flow in the entry region of the pipe. On the other hand, the laminar polymeric flow was found to be more stable than the Newtonian when subjected to an explicit finite amplitude forcing, a situation closer to the usual one which is unshielded from perturbations and yields transition at $Re \approx 2100$. These observations are consistent with the other observations of the usual transition [49, 59, 60]. Furthermore, they are consistent with the effects of viscoelasticity on the existence threshold for the exact coherent states described in Section 2.2 and below in Section 5.3. Specifically, viscoelasticity sharply increases the minimum Reynolds number at which these nontrivial solutions exist [62], so at a given Reynolds number, we expect the domain of attraction for the laminar solution to be larger for the viscoelastic flow than for the Newtonian, in agreement with the experiments.

The above discussions refer only to channels with smooth walls. Clearly, the strong coherence of the near wall vortices and streaks will be destroyed if the roughness height is comparable to the buffer layer thickness in the absence of roughness. Nevertheless, the mechanism driving strong streamwise vorticity – the tilting and stretching of vorticity into the mean flow direction by the mean shear – is still present. Detailed flow visualization (e.g. PIV) is difficult in the rough wall case, and to our knowledge has not yet been performed for a drag-reduced flow. For this reason and others, the phenomenology of drag reduction with rough walls does not seem to have been completely worked out. The pipe flow experiments of Spangler [63], for example, showed drag reduction that first increased, then peaked and decreased with increasing Reynolds number. The recent boundary layer experiments by Petrie *et al.*, [64], on the other hand, show no such decrease. A possible source of complications here is that not only the roughness height, but also its spatial structure on the surface may be important. Another is that the polymer increases the near-wall turbulent length scales, so measures of the roughness based solely on wall units do not

provide a full picture. Results described below, in Section 5.1, show that polymer additives suppress shear layer instabilities such as might appear in the wake of an individual roughness element in a strongly wave number dependent manner, with short wavelength instabilities very strongly suppressed but very long wavelength instabilities not suppressed at all. Experimentally, an example of the latter situation is provided by Cadot *et al.* [65]. They performed experiments where fluid in a cylindrical tank is stirred by a pair of counter-rotating impellers. Two different types of impellers were studied, smooth rimmed disks and baffled ones. The baffled disks provide inertial forcing (form drag) through what is basically outer scale roughness, while the smooth disks provide purely viscous forcing. Although similar behavior was seen in the core of the flow for the two cases, the level of drag in the viscously forced flow was substantially reduced by polymer, while the drag in the inertially forced case was largely unaffected. They argued based on these results that bulk turbulence, though modified by polymer, is not changed enough to lead to significant drag reduction, and that the reduction in energy dissipation is solely due to the near-wall behavior.

3.2 Direct numerical simulations of turbulent channel flow of polymer solutions

Detailed measurements of velocity fields in turbulent flow are difficult, even with Newtonian fluids. For polymer solutions, the situation is worse, with no direct experimental methods available for extracting spatially resolved information about polymer conformations. Furthermore, real drag-reducing polymer solutions are complex and difficult to rheologically characterize, especially with regard to extensional flow behavior. With recent advances in computational power and numerical methods has come the capability to perform detailed computational studies of flows of reasonably realistic polymer solution models at large Weissenberg numbers. In the context of drag reduction, most of these studies have been direct numerical simulations, solutions of the Navier-Stokes and polymer evolution equations as an initial value problem to directly compute turbulent flows of polymer solutions.

Some first attempts at “almost direct numerical simulation” were undertaken by Orlandi [66] and den Toonder *et al.* [67]. Orlandi simulated an inelastic model in which the extensional viscosity was large when the strain rate exceeded the vorticity and small otherwise, finding drag reduction accompanied by an increase in buffer layer streamwise fluctuations and a decrease in wall-normal fluctuations and streamwise vorticity, consistent with experimental observations at moderate drag reduction levels. Den Toonder *et al.* studied both inelastic and elastic models where the stress tensor depended on the local flow direction, i.e. $\tau_p \sim (\mathbf{u} \cdot \mathbf{D} \cdot \mathbf{u}) \mathbf{u} \mathbf{u} / (\mathbf{u} \cdot \mathbf{u})^2$, where \mathbf{u} is the velocity and \mathbf{D} the strain rate. This expression is motivated by the fact that orientable particles in a linear flow tend to align along the flow direction, and yielded similar results to those of Orlandi. These results suggest the importance of extensional stresses in drag reduction, but their interpretation is highly uncertain because neither constitutive equation is frame invariant [68].

The first simulations with a proper viscoelastic constitutive equation were reported by Sureshkumar, Beris and Handler [69]. They simulated channel flow using the FENE-P model for the polymer dynamics, as have most researchers since. In this

model, each polymer molecule is treated as a pair of beads connected by a finitely extensible non-linearly elastic (FENE) spring. All of the internal degrees of freedom of the polymer are lumped into the spring force model, and the Peterlin closure is applied to yield a closed form evolution equation for the conformation tensor [70]. The model has three parameters, λ , the stress relaxation time; β , the fraction of the zero-shear viscosity that is due to the polymer ($1-\beta$ is proportional to polymer concentration); and b , the polymer extensibility, which for chain of N Kuhn segments is given by $b = 3(N-1)$. A more directly relevant parameter than b is the quantity $2b(1-\beta)/3\beta$, which we denote Ex . This parameter is defined so that in uniaxial extension, Ex is the steady-state ratio between the polymer and solvent contributions to the stress in the limit of infinite extension rate. A significant effect of the polymer on the flow will only occur for $Ex \gg 1$. For long flexible polymers, Ex can be much greater than unity, even for very small concentrations, because b can be 10^4 or greater. (See Section 6 for more information on polymer models). A Fourier-Chebyshev-Fourier pseudo-spectral algorithm was used for spatial discretization, with an artificial diffusion term added to the equation for polymer conformation to maintain stability of the time-integration. To our knowledge in fact, all DNS studies of polymer turbulence have applied an artificial diffusivity, with a ‘‘Schmidt number’’, the ratio of momentum diffusivity to stress diffusivity, of $O(1)$, or some other *ad hoc* regularization, because of the difficulty of keeping the conformation tensor positive definite otherwise. A non positive-definite conformation tensor, in addition to being unphysical, leads to spurious instability in the momentum equation [71]. The regularization allows for simulations at very large Weissenberg numbers, and Sureshkumar *et al.* found that their simulations captured the experimental observed features of the moderate drag reduction regime (i.e. at Reynolds numbers above onset but not yet approaching maximum drag reduction. Specifically, they observed (at $Re_\tau=125$, $\beta = 0.9$, $Ex = 7.4$) an onset Weissenberg number We of about 10, an upward and outward shift of the near-wall mean velocity profile and streamwise fluctuations, decreases in the wall normal and spanwise fluctuations and Reynolds shear stress, and an increased streak spacing.

Based on these results, there can be little doubt that the FENE-P model has the essential ingredients of a drag-reducing fluid. Sureshkumar *et al.* also found a decrease in streamwise vorticity, especially in the wall region; furthermore, polymer stretch was found to peak in the buffer layer. In later work [72], the Beris group verified the importance of the parameter Ex in determining the features of drag reduction, and extended the simulations to the Giesekus model, confirming long standing views of the importance of extensional stresses for drag reduction. They also computed budgets of the Reynolds stress equations [73]. These closely corroborate the conclusions drawn by Walker and Tiederman [74] from their experimental studies, namely that the changes in the Reynolds stresses are tied closely to the velocity-pressure gradient correlation, which is in turn strongly affected by the near-wall vortices. In drag reduction, the streamwise vortices are weakened; the corresponding decrease in the pressure fluctuations decreases the (magnitude of the) velocity-pressure gradient term, and therefore reduces redistribution of turbulent kinetic energy from the streamwise to the other components. The most recent work from this group [75] revises the predicted onset Weissenberg number to about 6, and shows that for $Re_\tau \gtrsim 400$ the mean and fluctuation behavior in the wall region $y^+ < 100$ becomes virtually independent of Re_τ , varying only with We .

A number of other groups have performed similar studies, corroborating and extending the results of the Beris group. Sibilla and Baron [76] also examined the Reynolds stress budgets, again observing the suppression of redistribution of Reynolds stress in the buffer layer. De Angelis *et al.* [77] illustrated a strong anti-correlation in the buffer layer between the velocity fluctuations and the force exerted by the polymer on the fluid. In particular, they found the polymer force (i.e. the divergence of the polymer stress) to be largest in magnitude in the low speed streaks, the regions of slow moving fluid between the cores of the streamwise vortices. Min *et al.* [78] found similar results, interpreting them in terms of energy rather than force. They showed that at sufficiently large We , the polymer chains gain elastic energy very near the wall and can carry it into the buffer and lower log regions before releasing it by relaxing. (This is a rather indirect explanation for drag reduction, as it does not address how the relaxation in the vortices affects them. A more direct one is given below.) Eckhardt *et al.* [79] performed DNS of turbulent shear flow in the Couette geometry with free-slip boundary conditions on the deviations from the linear profile — roughly speaking, this eliminates the viscous sublayer from the flow. This is the only DNS study to date that explicitly addresses the relationship between polymer stretch and the largest Liapunov exponent (LLE) of the flow field — the asymptotic Lagrangian rate of material line stretching (cf. Section 4). They find that, at Weissenberg numbers such that polymers are not significantly stretched, the distribution of polymer extension has an algebraically decaying tail at high stretch, as predicted theoretically by Balkovsky *et al.* [80], with the power law exponent explicitly dependent on the LLE for the flow. Ptasincki *et al.* [81] have recently presented DNS results close to the maximum drag reduction asymptote, albeit for a small flow domain and unusually large polymer concentration. Their results generally corroborate experimental observations. In particular, they find a modified log layer slope close to what is observed experimentally, although it does not fill the channel under the conditions simulated. They also observe an initial increase, with later decrease of the streamwise velocity fluctuations upon increasing drag reduction, consistent with experiments [53, 55]. The Reynolds shear stress is strongly reduced, with the polymer stress compensating. One interesting result that had not been shown by earlier DNS studies was a breakdown in the self-similarity of correlation between motions near the wall and those closer to the centerline. Based in part on this observation the authors propose a heuristic mechanism for drag reduction, based on “shear sheltering”. No definitive test for this mechanism was performed or proposed, however. The Ptasincki *et al.* results near maximum drag reduction are corroborated by another recent DNS study, also in a quite small channel ($Re_\tau \approx 135$) by Min *et al.* [82].

In general, these studies contain no structural information about the flow other than snapshots of various single-point or ensemble-averaged quantities and in some cases, streak spacings. None of them has applied any type of pattern analysis methodology to the simulation results. The only study to date that has done this is that of de Angelis *et al.* [83], who used the Karhunen-Loève decomposition [84] to Newtonian and viscoelastic DNS results. This approach, which has been used widely for pattern analysis, both in fluid mechanics and elsewhere, finds a set of orthogonal modes, ordered by kinetic energy, such that a truncated expansion based on these modes retains the maximum fraction of the turbulent energy. In a well-defined sense, this is the optimal set of modes for representing the fluctuating component of the

velocity field. In the turbulence literature it is often called the “Proper Orthogonal Decomposition” [21, 85]. The most energetic modes are strongest near the wall, comprising a wavy streamwise vortex structure (see, e.g. [21, 22]). The main findings of de Angelis *et al.* are that (1) the spatial structures of the most energetic modes do not change significantly due to viscoelasticity, and (2) the fraction of kinetic energy captured by a given number of modes is larger in the viscoelastic case than in the Newtonian.

On the methodological side, Min *et al.* [86] and DuBief and Lele [87] have advocated the use of compact finite differences [88] rather than spectral discretizations for DNS of polymer solutions. The compact finite differences retain high accuracy in the context of a local rather than global discretization, thus minimizing the wiggles that arise in discretizations of functions with localized steep gradients. These wiggles can lead to non-positive definiteness of the polymer conformation tensor and thus to numerical instability. Vaithianathan and Collins [89] also used compact differences, and implemented an integration scheme for the polymer conformation tensor that enforced positive semi-definiteness without introducing an artificial stress diffusivity — any negative eigenvalues are set to zero at each time step. They applied their method not to channel flow, but to forced and decaying homogeneous isotropic turbulence. In the forced case they found a dramatic upturn in the energy spectrum in the polymer case at high Weissenberg numbers and extensibilities; whether this effect is physical or numerical remains unclear. In the decaying case they found “drag reduction” in the sense that viscoelasticity slows the decay of fluctuations. A similar result was experimentally found for grid turbulence of a polymer solution [90] but this turbulence remained markedly anisotropic throughout the decay.

4. KINEMATICS AND GENERAL CONSIDERATIONS FOR POLYMERS IN CHAOTIC AND TURBULENT FLOW FIELDS

An important concept from dynamical systems theory is that of Liapunov exponents. These are the time-averaged rates of separation of initially infinitesimally separated initial conditions, i.e. initially neighboring trajectories in the phase space of a differential equation. In the context of a flow field, they measure the Lagrangian time-averaged stretching rates of infinitesimal material lines. For a material line attached to a given trajectory, there are three Liapunov exponents σ , and the largest Liapunov exponent (LLE) will be denoted σ_{\max} . The relevance of the LLE for polymer dynamics is that to a first approximation, a polymer molecule in dilute solution undergoes affine deformation with the flow, modified by the constraint forces keeping the molecule together and the Brownian motion pushing it back toward equilibrium. For the simplest reasonable model of a polymer, a pair of beads connected by a Hookean spring — a Hookean dumbbell — a simple relationship between the polymer dynamics and the LLE can be derived. If the stress relaxation time for the dumbbell is λ , then the dumbbell will stretch exponentially rapidly in a given flow field if and only if $\lambda\sigma_{\max} > 1/2$. This result, a generalized “coil-stretch-transition” criterion, can be found in different form in [91]; a simple derivation of it is given in [92]. It is also shown in [92] that for detailed bead-spring-chain models of polymers for which no rigorous results are available, this result is still useful in that $\lambda\sigma_{\max} > 1/2$ signifies when the flow can stretch the chain to nearly full extension. Two-dimensional

bounded or periodic steady flows have $\sigma_{\max} = 0$ except for trajectories terminating at a hyperbolic stagnation point, while three-dimensional steady or time-dependent flows in a bounded or periodic domain can have chaotic trajectories, and thus $\sigma_{\max} > 0$, over much of the flow domain. Not surprisingly, DNS of isotropic homogeneous turbulence with a Kolmogorov time scale τ_K reveals a positive LLE: Girimaji and Pope [93] find $\sigma_{\max} 0.14/\tau_K$, while a recent, more precise calculation yields $\sigma_{\max} 0.17/\tau_K$ [94]. The ECS described above, though steady, have chaotic particle paths and thus $\sigma_{\max} > 0$ on most trajectories in the flow [62]. To our knowledge, Liapunov exponents have not been explicitly computed from DNS of channel flow. In this situation, where the stretching rates might be expected to vary dramatically with distance from the walls, the true Liapunov exponents will represent averages over regions with widely disparate local stretching rates. Here *finite time* Liapunov exponents may be more useful in determining whether local conditions are sufficient to stretch polymer molecules; these are simply the stretch rates averaged over a finite time, say the residence time of a fluid element in a particular region of the flow, rather than an infinite one.

Beginning with the relatively simple notion of Liapunov exponents and the coil stretch criterion $\lambda\sigma_{\max} = 1/2$, and using field-theoretic tools for treating random fields, recent progress has been made in developing some general results for polymers in random flow fields. Chertkov [95] and Balkovsky *et al.* [80, 96] showed that for a flow with $\lambda\sigma_{\max} < 1/2$, that the distribution of polymer stretch at a given point in the flow would have a power law tail, a result corroborated by the DNS of Eckhardt *et al.* [79]. Fouxon and Lebedev [97] have shown (under certain approximations) that the Fourier transform of the spatial correlation function of polymer stretch in a homogeneous isotropic random flow has a power law decay in wave number. A connection is drawn between this result and the dynamics of Alfvén waves in magneto-hydrodynamic systems — the magnetic field deforms with material lines, as do polymer molecules, and the stress tensor takes similar forms in the two cases, but dissipation of the magnetic field occurs by diffusion rather than by relaxation. Their results do not say anything specific about drag reduction but do predict an equipartition between kinetic energy and stored elastic energy in the polymer molecules. One might think of this last paper as an attempt to strengthen and extend the heuristic notion put forth by de Gennes [98] that polymer additives would suppress motions at the small length scales where the strain rates are high, cutting off the inertial range at a larger scale than in Newtonian flow.

The results discussed in the previous paragraph consider primarily the case $\lambda\sigma_{\max} \ll 1/2$, which may seem *a priori* like an irrelevant case. One can argue, however, that addition of long flexible molecules to turbulence will force the flow into a state with $\lambda\sigma_{\max} \approx 1/2$, as follows. (A similar argument is given in [96].) An effective drag reducer has $Ex \gg 1$, and will exert negligible stress on the solvent if $\lambda\sigma_{\max} \ll 1/2$. Recall that this parameter measures the maximum relative extensional stresses due to the polymer and the solvent. The maximum solvent extensional stress must be approximately equal to the maximum Reynolds stress; in particular, in the buffer layer the Reynolds and viscous stresses are comparable. Imagine that $\lambda\sigma_{\max}$ were to become $> 1/2$. Because $Ex \gg 1$, the extensional stresses due to the polymer would strongly resist extensional fluctuations, effectively killing the turbulence and dropping σ_{\max} to

zero. In other words, it seems likely that no balance of terms exists that can maintain $\lambda\sigma_{\max} \gg 1/2$ when $Ex \gg 1$. One further implication of this argument is that for $Ex \gg 1$, the polymer chains do not get stretched to full extension, except perhaps transiently in localized regions of the flow. In this situation, the non-linearity of the spring law will not be important, so the Oldroyd-B (Hookean spring force) model will give results equivalent to those from the FENE-P model. Min *et al.* [78] show an example of this equivalence. It also may be true, though this is not obvious, that the dynamics of the internal degrees of freedom are unimportant.

If this argument holds, the interesting question, then, is how the turbulence structure is modified to maintain a nontrivial balance between Reynolds and polymer stresses that leads to $\lambda\sigma_{\max} \approx 1/2$. A crude, non-mechanistic answer to this question is that the turbulent motions that stretch the polymers simply increase in length scale, thus having lower velocity gradients and thus lower stretching rates. This answer is consistent with experiment in some sense: the scales do increase upon onset of drag reduction, as pointed out above. However, the change in scale is not the only effect, as exemplified by the trends in the velocity statistics, which show not just an increase in scale but an increase in anisotropy at moderate degrees of drag reduction. Nevertheless, continuing with the crude argument about increase in scale, one could argue that MDR is attained when the scale of the polymer-stretching motions reaches the scale of the channel. Indeed, this idea is consistent with the observations of Virk that at MDR the “elastic layer” fills or nearly fills the channel, and with other observations described above. A related observation is made by Sreenivasan and White [99], in an examination of data made in light of their reformulation of the elastic theory of de Gennes [98]. In this impressionistic theory, the degree of extension of the polymer molecules is assumed to increase with decreasing length scale, for sufficiently small scales. Drag reduction is then said to arise by the attenuation of scales such that the polymer stress would be larger than the Reynolds stress. Sreenivasan and White modified this theory for pipe flow, and used experimental data to estimate the length scale for drag reduction based on their theory. At MDR, they found that this length scales with the pipe radius. This is not necessarily evidence in favor of the deGennes theory, however, and Sreenivasan and White are quite cautious in their conclusions; it has been observed directly from experimental data that the outer scale becomes important at large degrees of drag reduction so *any* model that contains a length scale that must be fit to data is likely to find that that length scale becomes the outer scale at large drag reduction.

5. INSIGHTS FROM MODEL FLOWS

Direct numerical simulation is a valuable tool for studying turbulence and drag reduction. Interpreting DNS results and extracting mechanistic insight from them can be difficult, because everything, important and superfluous, is going on all at once. At the other extreme, general theoretical arguments provide important qualitative insights are often very vague. It is thus desirable to consider well-defined models that allow detailed examination of specific phenomena that arise in turbulent flows. This section summarizes the results of several studies of such models.

5.1 Shear layer and wake instabilities

Azaiez and Homsy [100] and Hinch (who wrote Appendix E of Azaiez and Homsy) have examined theoretically the effect of viscoelasticity on the linear stability of a mixing layer with the classical hyperbolic tangent velocity profile. They examined three constitutive models for the polymer stresses, the Oldroyd-B, corotational Jeffreys and Giesekus models [68, 70]. For the Oldroyd-B fluid (FENE-P as $b \rightarrow \infty$), significant suppression of instability was observed. Although sufficiently long waves remain unstable, the wave number regime over which instability occurs is dramatically reduced, as is the maximum growth rate in the unstable regime. In the limit of long waves, Hinch showed that the stabilizing effect is due to the large stretching of polymer molecules in the center of the layer, which then acts as an elastic membrane, resisting the deformations required for instability. Long-wave perturbations are less strongly suppressed because an elastic membrane is more easily deformed by long-wavelength undulations than by short ones. A significant degree of stabilization was not observed for the corotational Jeffreys and Giesekus models, probably because they display unrealistically extreme shear-thinning for a dilute polymer solution. Rallison and Hinch [101] examined the related problem of the linear stability of a submerged jet of viscoelastic liquid governed by the Oldroyd-B model. In this case as well, viscoelasticity can suppress instability. Kumar and Homsy [102] extended the work of Azaiez and Homsy into the non-linear regime, examining the rollup of vortices in shear layers. Although their simulations were limited to very low values of polymer extensibility, at sufficiently large values of We/Re they found that the rollup process was inhibited.

These theoretical and computational results have been corroborated by recent experiments. Cadot and Kumar [103] studied instabilities of a wake produced by a circular cylinder in a uniform water flow with injection of viscoelastic fluid through holes pierced in the cylinder. They showed that the viscoelasticity drastically modified the instabilities: the two-dimensional Kelvin-Helmoltz-like instability giving rise to the Karman vortex street was found to be inhibited, the roll-up process appeared to be delayed and the wavelength of the street increased. These results are all consistent with the analyses. In a related experiment, Cressman *et al.* [104] studied the effect of viscoelasticity on the wake dynamics in a soap film, a nominally purely two-dimensional flow. They found that with addition of polymer the transverse velocity fluctuations in the wake were dramatically depressed, and rollup into a well-defined vortex street was shifted significantly downstream relative to the Newtonian case.

These results are relevant to turbulence and drag reduction in a variety of contexts. Wake instabilities driving turbulence fluctuations near a rough wall can be expected to be suppressed if the roughness scale is small enough for viscoelasticity to be effective. In contrast, large scale inertial forcing, e.g. by baffles as in the Cadot, Bonn and Douady [65] experiments drives very long wavelength instabilities, which are not affected by viscoelasticity. Indeed the experimental observation is that the long wavelength inertial forcing leads to no appreciable drag reduction. Bonn *et al.* [105] found experimentally that high vorticity filaments that are formed by roll-up of local shear layers are dramatically suppressed by addition of polymer. This observation is consistent with the rollup inhibition predicted by Kumar and Homsy. Finally, shear layer instability (of spanwise inflections) is part of the self-sustaining process

described above for near-wall quasi-streamwise vortices. So viscoelasticity suppresses part of this process (though it will be argued below that this is not the dominant effect).

5.2 Hairpin vortex formation

Vortex stretching is suppressed by viscoelasticity. Extensional flow is required to strongly stretch vortices and it is precisely these flows that are most strongly resisted by long flexible polymer molecules. Yarin [106] observed that the localized-induction approximation for line vortex dynamics can be generalized to include viscoelasticity. In this approximation, all of the viscoelasticity is concentrated in the vortex core and the polymer stress is purely extensional and tangent to the vortex axis - this situation is analogous to that found by Hinch at high Weissenberg number for the shear layer, where the effect of viscoelasticity is localized in a “membrane” in the shear layer. Using this new approximation, he studied the effect of viscoelasticity on the evolution of a vortex filament initially aligned in the spanwise direction, in a shear flow. Using the Oldroyd-B model, he found that viscoelasticity strongly altered the evolution of the filament, in some cases completely eliminating the horseshoe or hairpin vortices that evolve in the absence of viscoelasticity. These results are probably most relevant to events in the lower inertial layer where hairpins seem to be more prevalent than in the buffer layer, and in particular to observations that polymer additives may have some drag -reducing effect even before reaching the buffer layer. Finally, this model is actually a better model for injected polymer than for bulk polymer solutions, as injected polymer may persist in unmixed strings that are highly elastic, surrounded by a Newtonian background [103].

5.3 Exact coherent states

The importance of the buffer layer in turbulence production, and the changes in buffer layer brought about by polymer, have been emphasized in this review, and in much of the drag reduction literature. The existence of the “exact coherent states” described in Section 2.2 provides an opportunity to probe in a controlled way the effects of viscoelasticity on a model of the autonomous buffer layer dynamics. Using the FENE-P dumbbell model and computational bifurcation analysis, Stone, Waleffe and Graham have examined the influence of viscoelasticity on the Couette flow sinuous ECS [62, 92]. These states are Lagrangian chaotic, so material lines and thus polymer molecules will experience persistent exponential stretching. Significant effects are seen, therefore, even when the polymer contributes only a few percent of the shear viscosity. The effects of viscoelasticity on these coherent states were found to be very similar to those experimentally observed in the turbulent buffer layer during flow of polymer solutions. In particular, the Reynolds number at which these states come into existence is shifted upward by viscoelasticity, consistent with experimental observations of the effect of viscoelasticity on non-linear transition.

Another view of this increase in onset Reynolds number is that viscoelasticity increases the wall-normal length scale required for these states to sustain themselves, consistent with the observed increases in buffer layer scales in drag-reduced flows. (In

as yet unpublished work (Stone, Waleffe and Graham 2003), this upward shift is found to begin at $We \approx 6$, in close agreement to the onset Weissenberg number found recently for DNS of channel flow [75, 78]). The streamwise vorticity of the ECS decreases with increasing viscoelasticity, lowering the pressure fluctuations. Wall normal velocity fluctuations are significantly attenuated, while streamwise ones increase, except near the wall, where they decrease. Finally, the Reynolds shear stress decreases and drag is reduced, all in agreement with the experimentally observed trends.

The trends in the velocity fluctuations all follow from the suppression of the streamwise vortices, whose mechanism becomes apparent on examination of polymer stresses along fluid trajectories: polymer molecules stretch in (or moving into) the streak regions, remaining highly stretched until they begin to leave the streak. As molecules move from the streak into and around the vortices, they relax. The spatial gradients in stress, accompanying this relaxation, work against the vortices, “unwinding” them by tending to decelerate fluid elements as they move from streaks to vortices. (This scenario is quite similar to that put forth by Min *et al.* [78] and discussed above, but presented in terms of forces rather than energies.) The pressure field is dominated by the vortices, and because these are weaker in the viscoelastic case, the pressure fluctuations are smaller in the viscoelastic case than in the Newtonian. Therefore, the redistribution of Reynolds stress by the pressure-rate of strain tensor is altered, in the same way as found via DNS of full turbulence [73], resulting in the observed changes in the components of the Reynolds stress (Stone, Waleffe and Graham 2003, unpublished).

6. ADVANCES IN UNDERSTANDING DILUTE SOLUTION POLYMER DYNAMICS

Most theoretical and computational treatments of drag reduction are built upon very simple models for polymer molecules, such as the FENE-P model described above [68]. This model has one relaxation time and a one-to-one relationship between the end-to-end distance and the trace of the stress. It contains the essential qualitative elements that lead to drag reduction in polymer solutions and has become the model of choice for most computational studies of polymer solution fluid dynamics. Nevertheless, it is still desirable to know how faithful it is to the dynamics of real polymers, especially in the chaotic environment of a turbulent flow.

The groundwork for theoretically addressing this issue was laid in two papers that appeared in 1978, by Fixman [107] and Ermak and McCammon [108]. These papers independently showed how to perform “Brownian dynamics” simulations of the stochastic differential equations that describe the large-scale motions of macromolecules in a solvent. Liu [109] used Brownian dynamics to study the dynamics of a freely jointed chain in flow, neglecting hydrodynamic interactions between chain segments. Doyle *et al.* [110], extended this work and made explicit comparisons between the freely jointed chain model with 100 segments and the FENE-P model. Petera and Muthukumar [111] added hydrodynamic interactions, using an algorithm developed by Öttinger [112]. The freely jointed chain model is a rather fine-grained model — each segment is a Kuhn length. A typical drag reducing

polymer molecule, say polyethylene oxide, might be more than 10000 Kuhn lengths long, making this model impractical for detailed computations. A more coarse-grained model is the bead-spring chain model; typically the FENE spring force is used for each spring. Many studies have been undertaken with this model; with the use of an approximation proposed by Fixman [113], it has become feasible to incorporate hydrodynamic interactions and study chains of 100 or more beads [114]. Using such simulations, it is found that the high Weissenberg number scalings of the shear viscosity and first normal stress coefficient are close to those of the FENE-P model [115]. Hsieh *et al.* [116] provide a good discussion of issues arising of coarse-graining to the bead-spring chain level, especially with regard to hydrodynamic interactions.

Bead-spring chain models have been used to study polymer dynamics in model turbulent flow fields. In all the cases described here, there is no effect of the polymer on the flow; the flow field is fixed. Massah and co-workers performed simulations of FENE bead-spring chains in a flow field obtained from direct numerical simulation of Newtonian turbulent channel flow and found that when the Weissenberg number We exceeds a certain threshold, the transient polymer stretch is significantly larger than its coiled equilibrium length [117]. Later work by the same group found that the stresses introduced by the stretched polymers in a turbulent flow lead to added dissipations, both positive and negative, in the buffer layer [118]. The positive dissipations are associated with the streamwise vortices in the near-wall region and would decrease the production of Reynolds stress in these structures. Recent work by Ilg *et al.* [119] addressed the dynamics of FENE and FENE-P dumbbells in wall turbulent flow. The flow field was taken from a fully coupled DNS of a drag-reducing (FENE-P) polymer solution. They found that the dumbbells become highly stretched in near-wall turbulence and highly oriented toward the mean flow direction. Comparison of the Lagrangian averages of the FENE and FENE-P cases shows that the extensions are qualitatively similar, with the FENE-P model giving slightly greater extension when velocity gradients are high and polymers are highly stretched. The stretching of an ensemble of FENE dumbbells integrated along the same trajectory in the flow is characterized by a broad (instantaneous) distribution of polymer extensions. None of these studies incorporated hydrodynamic interaction or excluded volume effects. Stone and Graham [92] have studied bead-spring chain dynamics, including these effects, in the flow field of a Couette flow exact coherent state described in Sections 2.2 and 5.3. The chains become highly stretched in the streamwise streaks and relax as they move into and around the vortex cores, leading to large differences in stress in different regions of the flow. Recall that it is this relaxation that leads to the weakening of the streamwise vortices. At the chain lengths and degrees of discretization studied, hydrodynamic and excluded volume interactions between polymer segments were found to have no qualitative effects once results were normalized for the change in relaxation time due to their inclusion. Most importantly, large polymer stress in the flow is seen at the same spatial positions for both the FENE-P and the more detailed models. The results from the bead-spring chain models were used to assess the utility of the simpler FENE-P model.

One of the known deficiencies of the FENE-P model is that FENE-P does not show “stress hysteresis” [120, 121]. For real polymers two conformations with the same end-to-end distance can have different internal configurations, leading to different values of stress. In the FENE-P model, the stress depends only upon the

current end-to-end distance so this hysteresis is not present. In the ECS flow field, the simulations with the full chain model clearly show hysteresis; the stress *vs.* extension curve for the FENE-P model lies slightly (a factor of two or less) below the rough hysteresis loop traced out by the chain model, suggesting that the FENE-P will yield slightly conservative estimates of the magnitude of the drag reduction effect. Although the FENE-P model does not capture the hysteresis in stress that is seen with the bead-spring chain models, it otherwise qualitatively captures the behavior of the bead-spring chains. Ghosh *et al.* [122] have proposed a modification to the FENE-P model that allows for stress-conformation hysteresis; it will be interesting to see how results with this model compare to chain simulations. Zhou and Akhavan [123], after performing a similar comparison to that of Stone and Graham, but for chains in the flow field of a Newtonian DNS simulation, drew much less optimistic conclusions regarding the FENE-P model. Nevertheless, the differences found in that work are quantitative, not qualitative, and use of the FENE-P model seems unlikely, based on current knowledge, to lead to qualitatively incorrect conclusions regarding mechanisms of drag reduction.

This discussion has given short shrift to the role of experiments in advancing our knowledge of dilute solution polymer dynamics. In the context of drag reduction, extensional rheometry is perhaps the most important experimental tool for studying dilute solutions. We refer the reader to the recent review by McKinley and Sridhar [48] for a survey of recent progress in this area.

Finally, the theory of dilute solution polymer dynamics in flow is at present only well-developed for the case of extremely dilute solutions of non-interacting polymer molecules. The possibility of polymer aggregation during a drag-reduced turbulent flow was realized some time ago (Lumley's 1969 review [7] mentions this issue), but the role of this phenomenon in drag reduction is unknown. Larson [124] has reviewed the general area of flow-induced phase transitions in flowing polymer solutions, and several commonly studied water soluble drag reducing polymers, polyacrylamide, partially hydrolyzed polyacrylamide and polyethylene oxide, are all known to aggregate in shear flow [125].

7. CONCLUSIONS

Near-onset drag reduction in flows with smooth walls is reasonably well-understood. Once the strain rate at the wall is significantly larger than the polymer relaxation rate, polymer chains stretch in the near-wall streaks and do not relax until they enter the quasi-streamwise vortices, suppressing them. It is these streamwise vortices in the buffer layer that drive convective momentum transport; suppressing them reduces drag. In addition, the decrease in the strength of these vortices affects the redistribution of Reynolds stress, leading to the observed changes in the buffer layer velocity fluctuations. It seems likely that a related mechanism may also act in the log layer, as well, as the mean shear flow tilts and stretches vorticity into the mean flow direction. Because the strain rates are lower here, however, the polymers are not as highly stretched and their influence is weaker than it is in the buffer region. Some light might be shed on this issue by DNS of viscoelastic homogeneous turbulent shear flow.

Direct numerical simulations of channel flow with simple polymer models capture and illuminate the key experimental observations in this regime.

The existence of exact coherent states — time-periodic, traveling wave solutions to the Navier Stokes equations that reproduce near-wall structure — shows that the dynamics of the buffer region are autonomous. These states are affected in the near onset regime by viscoelasticity in the same manner as is full turbulence. The effects of viscoelasticity on the onset of these states accords with experimental observations, providing further evidence that these states also underlie transition to turbulence, although research is still necessary to better establish the relationship between these flows and full turbulence. In addition to suppressing the quasi-streamwise vortex exact coherent states, viscoelasticity suppresses, through mechanisms that are basically understood, the shear layer instabilities, wake instabilities and hairpin vortex formation (and more generally, vortex stretching) processes that underlie turbulence production in many situations, including turbulence over rough or structured walls. Nevertheless, significant questions remain in these situations. In general the question of the “mechanism” of drag reduction becomes one of which processes in a flow are the most effective at rapidly stretching material lines.

We do not understand the dominant processes that occur at large levels of drag reduction, near the maximum drag reduction asymptote. What is clear is that the polymer dynamics are affecting scales up to the outer scale and that the distinction between inner and outer scaling is lost — the “near-wall” regime may no longer be near the wall. Experiments, especially PIV observations, will play an important role in the resolution of this issue. DNS is beginning to be capable of probing this regime, but with straightforward DNS it remains challenging to disentangle what is essential to the turbulence and drag reduction process from what is consequential. An important theoretical question is the role of exact coherent states, if any, in the MDR regime. Do they remain in existence or are they completely suppressed, allowing some other flow structures to become dominant? Is there a singularity at a finite We , beyond which these states do not exist at any Reynolds number? Is there, for every finite channel size (Re_τ), a Weissenberg number beyond which these structures cannot exist?

One possibility is that the sinuous – staggered quasistreamwise vortex – class of ECS that has been studied to date is killed by viscoelasticity, but that there exist other types of coherent traveling wave states (hairpins, Tollmien-Schlichting waves,...) that are only weakly affected by viscoelasticity and survive to become relevant sources of turbulence production in the MDR regime. In other words, there may be motions that are viable in Newtonian flow but are only unmasked as viscoelasticity suppresses the dominant Newtonian processes. Figure 1 schematically illustrates this hypothetical scenario. It shows the minimum wall normal thickness Δy_{\min}^+ required for a given flow pattern to be self-sustaining, as a function of Re_τ . For a given polymer solution, $Re_\tau = (We H^2/\lambda\nu)^{1/2}$. A structure only “fits” in a given channel if its Δy_{\min}^+ lies below the line $\Delta y_{\min}^+ = Re_\tau$. Curve ECS-S represents the existence boundary for the sinuous ECS. In the diagram, we have hypothesized that the sinuous only exist in a given channel over a certain interval in Re_τ . The left edge of the interval (i.e. the left intersection of ECS-S and the line $\Delta y_{\min}^+ = Re_\tau$) corresponds to transition to turbulence. At the high We end we have drawn two possibilities. The first is “blowup” – the curve increases beyond the $\Delta y_{\min}^+ = Re_\tau$ curve, so in this case the

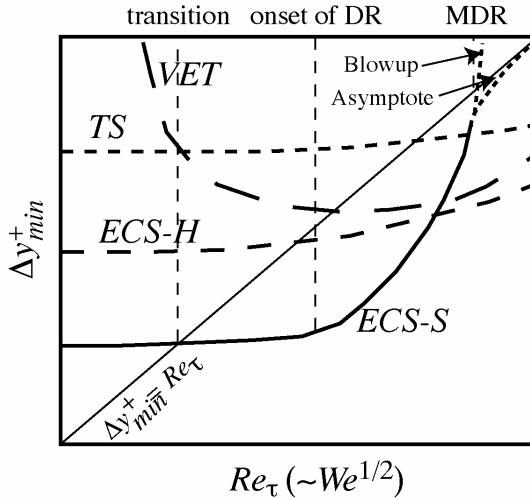


Figure 1: Schematic of a structure-based model for turbulent drag reduction. Labels are defined in the text. A state only fits in the channel when its existence region lies below the diagonal line. Two possible behaviors of the ECS-S curve, “blowup” and “asymptote” are shown, as discussed in the text.

sinuous ECS can no longer fit in the channel and are not observed. Also shown on the plot are two other hypothesized curves, one for Tollmien-Schlichting waves, TS, (we know that this curve exists, but not yet what it looks like), and another, more conjectural one, for an as-yet undiscovered class of ECS that have the spanwise reflection symmetry of hairpin vortices (ECS-H). In the schematic, these curves lie below the line $\Delta y_{min}^+ = Re_{\tau}$, indicating that they fit in the channel in the MDR regime and would be driving forces for turbulent fluctuations there. In reality, one or both of these curves might fit in the channel. Or perhaps these states are not relevant at all, and the polymer dynamics is driving new types of inherently viscoelastic turbulent motions. Such states might appear as the curve VET on Figure 1. Finally, we point out the much simpler possibility, that at high We the ECS-S curve does *not* cross the $\Delta y_{min}^+ = Re_{\tau}$ curve at all, but rather asymptotes to it, remaining in existence at arbitrarily large We . If this is the case, understanding the high We asymptotics of the sinuous ECS will shed significant light on the mechanism underlying MDR.

Our understanding of the dynamics of individual highly flexible polymer molecules in dilute solution is approaching maturity. Nevertheless, there are many coarse-graining issues still to confront in constructing simple few-degree-of-freedom models of such molecules in flow. Polymer aggregation in flow needs to be better understood, both in terms of its molecular features and its role in drag reduction. This issue is related to the behavior of micellar surfactant systems in flow. It is thought by

many researchers that the large extensional stresses that can arise in these solutions stem from flow-induced aggregation of the micelles into very long bundles or some other structure [126], and that this phenomenon accounts for the very strong drag-reducing properties of these materials. For other drag reducing additives like bubbles or fibers, the modeling situation is changed by the fact that these additives can have the same size as the important turbulence scales — indeed this fact may account in part at least for their effectiveness. Synergies have been observed between the drag reducing properties of various additives; the origins, rheological and/or fluid mechanical, of these synergies are of fundamental interest.

ACKNOWLEDGEMENTS

The author's work in polymer dynamics and drag reduction has been supported by the National Science Foundation and the Petroleum Research Fund of the American Chemical Society. Professor Fabian Waleffe has been an invaluable collaborator in this work, as have Philip Stone and Richard Jendrejack.

REFERENCES

1. Toms B A, Proceedings of the International Congress on Rheology, North-Holland, 1949.
2. Toms B A, *Phys. Fluids*, 20 (1977) S3-S8.
3. Mysels K J, U.S. Patent 2, 492, 173, (1949).
4. Mysels K J, *Early experiences with viscous drag reduction*, Drag Reduction: Chemical Engineering Progress Symposium Series, Vol. 67, Number 11, (1972).
5. McComb W D, "The Physics of Fluid Turbulence," Oxford University Press, New York, (1990).
6. Gyr A and Bewersdorff H-W, "Drag Reduction of Turbulent Flows," Kluwer, (1995).
7. Lumley J L, *Annu. Rev. Fluid Mech.*, 1 (1969) 367-384.
8. Lumley J L, *J. Polymer Sci.: Macromolec. Revs.*, 7 (1973) 263-290.
9. Virk P S, *AIChE J.*, 21 (1975) 625-655.
10. Berman N S, *Annu. Rev. Fluid Mech.*, 11 (1978) 47-64.
11. Shenoy A V, *Colloid and Polymer Sci.*, 262 (1984) 319-337.
12. Drag Reduction: Chemical Engineering Progress Symposium Series, Vol. 67, Number 11, (1972).
13. IUTAM Symposium on Structure of Turbulence and Drag Reduction, *Phys. Fluids* vol. 20, No. 10, part II, (1977).
14. The influence of polymer additives on velocity and temperature fields: IUTAM Symposium Essen 1984, Springer-Verlag, (1985).

15. Nadolink R H and Haigh W W, ASME Appl. Mech. Rev., 48 (1995) 351-460.
16. Bird R B, Stewart W E and Lightfoot E N, "Transport Phenomena," Wiley, New York, (1960).
17. Pope S B, "Turbulent Flows," Cambridge, (2000).
18. Sreenivasan K R, *A unified view of the origin and morphology of the turbulent boundary layer structure*, in Turbulence Management and Relaminarization, Springer, (1988).
19. Wei T and Willmarth W W, J. Fluid Mech., 204 (1989) 57-95.
20. Robinson S K, Annu. Rev. Fluid Mech., 23 (1991) 601-639.
21. Holmes P, Lumley J L and Berkooz G, "Turbulence, Coherent Structures, Dynamical Systems and Symmetry and Symmetry," Cambridge, (1996).
22. Webber G A, Handler R A and Sirovich L, Phys. Fluids, 9 (1997) 1054-1066.
23. Jeong J, Hussain F, Schoppa W and Kim J, J. Fluid Mech., 332 (1997) 185-214.
24. Zhou J, Meinhardt C D, Balachandar S and Adrian R J, *Formation of coherent hairpin packets in wall turbulence*, in Self-Sustaining Mechanisms of Wall Turbulence, Computational Mechanics Publications, (1997).
25. Kim K C and Adrian R J, Phys. Fluids, 11 (1999) 417-422.
26. del Alamo J C and Jimenez J, Phys. Fluids, 15 (2003) L41-L44.
27. "Self-sustaining mechanisms of wall-turbulence", Panton R L (Editor), Computational Mechanics Publications, (1997).
28. Swearingen J D and Blackwelder R F, J. Fluid Mech., 182 (1987) 255-290.
29. Nagata M, J. Fluid Mech., 169 (1986) 229-250.
30. Nagata M, J. Fluid Mech., 188 (1988) 585-598.
31. Nagata M, J. Fluid Mech., 217 (1990) 519-527.
32. Clever R M and Busse F H, J. Fluid Mech., 344 (1997) 137-153.
33. Waleffe F, Phys. Rev. Lett., 81 (1998) 4140-4143.
34. Waleffe F, J. Fluid Mech., 435 (2001) 93-102.
35. Waleffe F, Phys. Fluids, 15 (2003) 1517-1534.
36. Faisst H and Eckhardt B, Phys. Rev. Lett. 91 (2003) 22450.
37. Strogatz S H, "Non-linear Dynamics and Chaos: With Applications to Physics, Biology, Chemistry and Engineering," Addison Wesley, (1994).
38. Daviaud F, Hegseth J and Berge P, Phys. Rev. Lett., 69 (1992) 2511-2514.
39. Bottin S, Dauchot O, Daviaud F and Mannville P, Phys. Fluids, 10 (1998) 2597-2607.
40. Hamilton J M, Kim J and Waleffe F, J. Fluid Mech., 287 (1995) 317-348.

41. Waleffe F, *Phys. Fluids*, 9 (1997) 883-900.
42. Jimenez J and Pinelli A, *J. Fluid Mech.*, 389 (1999) 335-359.
43. Jimenez J and Moin P, *J. Fluid Mech.*, 225 (1991) 213-240.
44. Guckenheimer J and Holmes P, "Non-linear Oscillations, Dynamical Systems and Bifurcations of Vector Fields," Springer, New York, corrected second printing, (1986).
45. Kawahara G and Kida S, *J. Fluid Mech.*, 449 (2001) 291-300.
46. Toh S and Itano T, *J. Fluid Mech.*, 481 (2003) 67-76.
47. Jimenez J and Simens M P, *J. Fluid Mech.*, 435 (2001) 81-91.
48. McKinley G H and Sridhar T, *Annu. Rev. Fluid Mech.*, 34 (2002) 375-415.
49. Escudier M P, Presti F and Smith S, *J. Non-Newtonian Fluid Mech.*, 81 (1999) 197-213.
50. Berman N S, *Phys. Fluids*, 20 (1977) S168-S174.
51. Zakin J L, Myska J and Chara Z, *AIChE J.*, 42 (1996) 3544-3546.
52. Donohue G L, Tiederman W G and Reischman M M, *J. Fluid Mech.*, 56 (1972) 559-575.
53. Warholic M D, Heist D K, Katcher M and Hanratty T J, *Exp Fluids*, 31 (2001) 474-483.
54. White C M, Somandepalli V S R and Mungal M G, *Expts. Fluids*, (2003) online article.
55. Ptasiński P K, Nieuwstadt F T M, van den Brule B H A A and Hulsen M A, *Flow, Turbulence and Combustion*, 66 (2001) 159-182.
56. Warholic M D, Massah H and Hanratty T J, *Exp Fluids*, 27 (1999) 461-472.
57. McComb W D and Rabie L H, *AIChE J.*, 28 (1982) 547-557.
58. McComb W D and Rabie L H, *AIChE J.*, 28 (1982) 558-565.
59. Giles W B and Pettit W T, *Nature*, 216 (1967) 470-472.
60. White W D and McEligot D M, *ASME J. Basic Engineering*, 92 (1970) 411-418.
61. Draad A A, Kuiken G D C and Nieuwstadt F T M, *J. Fluid Mech.*, 377 (1998) 267-312.
62. Stone P A, Waleffe F and Graham M D, *Phys. Rev. Lett.*, 89 (2002) 208-301.
63. Spangler J, *Studies of viscous drag reduction with polymers including turbulence measurements and roughness effects*, in *Viscous Drag Reduction*, Plenum, (1969).
64. Petrie H L, Deutsch S, Brungart T A and Fontaine A A, *Expts. Fluids*, 35 (2003) 8-23.

65. Cadot O, Bonn D and Douady S, *Phys. Fluids*, 10 (1998) 426-436.
66. Orlandi P, *J. Non-Newtonian Fluid Mech.*, 60 (1995) 277-301.
67. den Toonder J M J, Hulsen M A, Kuiken G D C and Nieuwstadt F T M, *J. Fluid Mech.*, 337 (1997) 193-231.
68. Bird R B, Armstrong R C and Hassager O, "Dynamics of Polymeric Liquids," vol. 1, Wiley, New York, (1987).
69. Sureshkumar R, Beris A N and Handler R A, *Phys. Fluids*, 9 (1997) 743-755.
70. Bird R B, Curtiss C F, Armstrong R C and Hassager O, "Dynamics of Polymeric Liquids," vol. 2, Wiley, New York, (1987).
71. Dupret F and Marchal J M, *J. Non-Newtonian Fluid Mech.*, 20 (1986) 143-171.
72. Dimitropoulos C D, Sureshkumar R and Beris A N, *J. Non-Newtonian Fluid Mech.*, 79 (1998) 433-468.
73. Dimitropoulos C D, Sureshkumar R, Beris A N and Handler R A, *Phys. Fluids*, 13 (2001) 1016-1027.
74. Walker D T and Tiederman W G, *J. Fluid Mech.*, 218 (1990) 377-403.
75. Housiadas K D and Beris A N, *Phys. Fluids*, 15 (2003) 2369-2384.
76. Sibilla S and Baron A, *Phys. Fluids*, 14 (2002) 1123-1136.
77. Angelis E D, Casciola C M and Piva R, *Computers and Fluids*, 31 (2002) 495-507.
78. Min T, Yoo J Y, Choi H and Joseph D D, *J. Fluid Mech.*, 486 (2003) 213-238.
79. Eckhardt B, Kronjager J and Schumacher J, *Comput. Phys. Comm.*, 147 (2002) 538-543.
80. Balkovsky E, Fouxon A and Lebedev V, *Phys. Rev. Lett.*, 84 (2000) 4765-4768.
81. Ptasinski P K, Boersma B J, Nieuwstadt F T M, Hulsen M A, van den Brule B H A A and Hunt J C R, *J. Fluid Mech.*, 490 (2003) 251-291.
82. Min T, Choi H and Yoo J Y, *J. Fluid Mech.*, 492 (2003) 91-100.
83. Angelis E D, Casciola C M, L'vov V S, Piva R and Procaccia I, *Phys. Rev. E*, 67 (2003) 056312.
84. Fukunaga K, "Introduction to Statistical Pattern Recognition," Academic Press, New York, (1990).
85. Lumley J L, "Stochastic Tools in Turbulence," Academic Press, New York, (1970).
86. Min T, Yoo J Y and Choi H, *J. Non-Newtonian Fluid Mech.*, 100 (2001) 27-47.
87. Dubief Y and Lele S K, "Direct numerical simulation of polymer flow," Center for Turbulence Research Annual Research Briefs, (2001).

88. Lele S K, *J. Comp. Phys.*, 103 (1992) 16-42.
89. Vaithianathan T and Collins L R, *J. Comput. Phys.*, 187 (2003) 1-21.
90. van Doorn E, White C M and Sreenivasan K R, *Phys. Fluids*, 11 (1999) 2387-2393.
91. Lumley J L, *Symp. Math.*, 9 (1972) 315-334.
92. Stone P A and Graham M D, *Phys. Fluids*, 15 (2003) 1247-1256.
93. Girimaji S S and Pope S B, *J. Fluid Mech.*, 220 (1990) 427-458.
94. Kida S and Goto S, *Phys. Fluids*, 14 (2002) 352-361.
95. Chertkov M, *Phys. Rev. Lett.*, 84 (2000) 4761-4764.
96. Balkovsky E, Fouxon A and Lebedev V, *Phys. Rev. E*, 64 (2001) 056301.
97. Fouxon A and Lebedev V, *Phys. Fluids*, 15 (2003) 2060-2072.
98. de Gennes P-G, "Introduction to Polymer Dynamics," Cambridge University Press, New York, (1990).
99. Sreenivasan K R and White C M, *J. Fluid Mech.*, 409 (2000) 149-164.
100. Azaiez J and Homay G M, *J. Fluid Mech.*, 268 (1994) 37-69.
101. Rallison J M and Hinch E J, *J. Fluid Mech.*, 288 (1995) 311-324.
102. Kumar S and Homay G M, *J. Non-Newtonian Fluid Mech.*, 83 (1999) 249-276.
103. Cadot O and Kumar S, *J. Fluid Mech.*, 416 (2000) 151-172.
104. Cressman J R, Bailey Q and Goldburg W I, *Phys. Fluids*, 13 (2001) 867-871.
105. Bonn D, Couder Y, van Dam P J H and Douady S, *Phys. Rev. E*, 47 (1993) R28-R31.
106. Yarin A L, *J. Non-Newtonian Fluid Mech.*, 69 (1997) 137-153.
107. Fixman M, *J. Chem. Phys.*, 69 (1978) 1527-1537.
108. Ermak D L and McCammon J A, *J. Chem. Phys.*, 69 (1978) 1352-1359.
109. Liu T W, *J. Chem. Phys.*, 90 (1989) 5826-5842.
110. Doyle P, Shaqfeh E S G and Gast A P, *J. Fluid Mech.*, 334 (1997) 251-291.
111. Petera D and Muthukumar M, *J. Chem. Phys.*, 111 (1999) 7614-7623.
112. Öttinger H-C, *Phys. Rev. E*, 50 (1994) 2696-2701.
113. Fixman M, *Macromolecules*, 19 (1986) 1204-1207.
114. Jendrejack R M, Graham M D and de Pablo J J, *J. Chem. Phys.*, 113 (2000) 2894-2900.
115. Jendrejack R M, de Pablo J J and Graham M D, *J. Chem. Phys.*, 116 (2002) 7752-7759.

116. Hsieh C C, Li L and Larson R G, *J. Non-Newtonian Fluid Mech.*, 113 (2003) 147-191.
117. Massah H, Kontomaris K, Schowalter W R and Hanratty T J, *Phys. Fluids A*, 5 (1993) 881-890.
118. Massah H and Hanratty T J, *J. Fluid Mech.*, 337 (1997) 67-101.
119. Ilg P, De Angelis E, Karlin I V, Casciola C M and Succi S, *Europhys. Lett.*, 58 (2002) 616-622.
120. Larson R G, "Constitutive Equations for Polymer Melts and Solutions," Butterworths, Boston, (1988).
121. Ghosh I, McKinley G H, Brown R A and Armstrong R C, *J. Rheol.*, 45 (2001) 721-758.
122. Ghosh I, Joo Y L, McKinley G H, Brown R A and Armstrong R C, *J. Rheol.*, 46 (2002) 1057-1089.
123. Zhou Q and Akhavan R, *J. Non-Newtonian Fluid Mech.*, 109 (2003) 115-155.
124. Larson R G, *Rheol. Acta*, 31 (1992) 497-520.
125. Liberatore M W, Pollauf E J and McHugh A J, *J. Non-Newtonian Fluid Mech.*, 113 (2003) 193-208.
126. Walker L M, *Curr. Opin. Coll. Int. Sci.*, 6 (2001) 451-456.